Molecular Dynamics (MD) Simulations and Large-Angle X-ray Scattering (LAXS) Studies of the Solid-State Structure and Assembly of Isotactic (*R*)-Poly(2,2′-dioxy-1,1′-binaphthyl-)phosphazene in the Bulk State and in the Cast Film

Gabino A. Carriedo,[b] Francisco J. García Alonso,[b] José L. García Alvarez,[b] Giuseppe M. Lombardo,[a] Giuseppe C. Pappalardo,*[a] and Francesco Punzo[a]

Abstract: The intrachain conformation, molecular structure and interchain assembly of isotactic (*R*)-poly(2,2′-dioxy-1,1′-binaphthyl)phosphazene (P-DBNP) both in the bulk state (I) and in the cast film (II) were studied by molecular dynamics (MD) simulations of models, as implemented by a bias potential for the analysis of the radial distribution function (RDF) obtained from large-angle X-ray scattering (LAXS) data. The microscopic structure and order extension of the polymer changed from I to II, as qualitatively shown in the shapes of their experimentally measured RDF curves. With the use of a bias potential, the MD simulations provided a much more accurate analysis of the models, as seen in the reproduction of the RDFs. The chiral P-DBNP chain was found to be consistent with helix conformations in both the I and the II samples. The predominant interchain clustering motif was best reproduced with a seven-chain model. In the case of I, the maximum chain length was 18 monomeric $-R_2NP-$ units, while in the case of the cast film II the chain was more elongated, up to distances of approximately 100 Å, equivalent to over 48 monomeric $-R_2NP-$ units. The seven-chain assembly was accounted for in terms of nonbonded interactions favouring the minimum voids area between the seven tubular structures of the material. The results validate our earlier finding that MD analysis with implementation of a biasing potential for the RDFs can provide quantitative information on the structural and conformational features of amorphous solids. The combined theoretical and experimental approach was found to be a useful tool to detect, locate and evaluate the intra- and intermolecular modifications of materials subsequent to their phase transformation and, as in the present case, changes in their microscopic structures or preparation methods.

Keywords: molecular dynamics · polyspirophosphazenes · structure elucidation · X-ray diffraction

Introduction

Linear polyphosphazenes are inorganic macromolecules made up of $-R_2PN-$ units, in which R may be halogen, pseudo-halogen, alkoxy, aryloxy, amino, alkyl or aryl groups. During recent decades the chemistry, properties and applications of polyphosphazenes—as, inter alia, elastomers, fire-retardant agents, membranes or biocompatible polymers—have been extensively studied and reviewed.[1–4] Recently, the growing progress in the synthetic methods for this type of polymers has given rise first to the novel high molecular weight derivatives with 2,2′-dioxybiphenyl-phosphazene repeating units $[NP(O_2C_{12}H_8)]_n$ (poly-spirophosphazenes)[5] and, finally, to their 2,2′-dioxy-1,1′-binaphthyl-phosphazene analogues $[NP(O_2C_{20}H_{12})]_n$ (see below), here denoted as P-DBNP, which could be obtained as isotactic *R* or *S* polymers, or as (*R*/*S*)-copolymers[6] (see below) with different proportions of both chiral units.

The study of the structure and molecular assembly of P-DBNP both as a powder (I) and as a film (II) is helpful for understanding of the stereochemistry of functionalised copolymeric derivatives of the type $\{[NP(O_2C_{20}H_{12})]_{1-x}[NP(OC_6H_5R)_2]_x\}_n$[6–9]. These systems may have helicoidal conformations with the R groups immersed in chiral pockets,[9] and so they are interesting as synthetic helical polymers[10] and potentially useful as supported catalysts for enantiomer-

[a] Dr. G. M. Lombardo, Prof. G. C. Pappalardo, Dr. F. Punzo
Dipartimento di Scienze Chimiche
Cattedra di Chimica Generale, Facoltà di Farmacia
Università di Catania, Viale A. Doria 6
95125 Catania (Italy)
Fax: (+39) 095-337-751
E-mail: gcpappalardo@dipchi.unict.it

[b] Prof. G. A. Carriedo, Prof. F. J. G. Alonso, Dr. J. L. G. Alvarez
Departamento de Química Orgánica y Inorganica
Universidad de Oviedo, Oviedo 33071 (Spain)

 DOI: 10.1002/chem.200400051

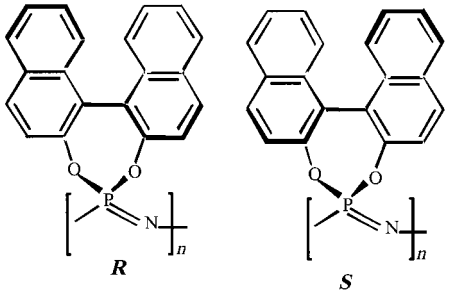

R *S*

$[NP(O_2C_{20}H_{12}]_n$

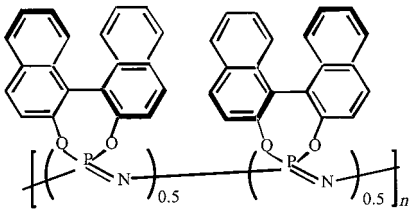

R/S

ic synthesis.[11] Obtaining information on the structural and conformational features of these polymers is also a central issue in studies focused on the technological applications of these materials. Of particular concern are the structure–property relationships, which need to be better understood in terms of both intrachain and interchain interactions and ordering that might give rise to molecular recognition.

The major impediment to the obtaining of detailed information about the structure, conformation and molecular arrangement of poly-spirophosphazenes is the fact that they are amorphous, or, at the best, of low crystallinity. The lack of translation symmetry makes the application of classical X-ray diffraction techniques—so straightforward for crystalline materials—difficult or impossible in these systems.

Acquisition of structural information for a given material independent of its degree of molecular ordering is a current challenge. This study is an endeavour to solve this experimental problem with computational techniques.

Molecular dynamics (MD), combined with large angle X-ray scattering (LAXS) and with NMR spectroscopy, has recently been used by us for the determination of structural parameters (molecular assembly, interatomic and intermolecular distances) in the bulk,[3,12–14] and of stereochemistry in solution,[15] respectively, of phosphazenic systems. Energy dispersive X-ray diffraction (EDXD) is a LAXS modification that has been recognized to be useful for rapid derivation of the coherent scattering intensity curve.[16–18]. The MD technique has been shown to be a suitable way to assess the local structural order from the radial distribution function (RDF) curve.[3,12–14] The shape (peak positions and intensity) of the measured RDF curve can be reproduced by the calculated RDF from "snapshots" collected along the entire evolution time of the MD simulation of each model considered. Comparison between experimentally determined and theoretical RDFs can provide information not only on the structures but also on the dynamic properties of the system.

The measured RDF for a polymer represents a weighted sum of atom–atom distributions. To assess the origin of the RDF quantitatively, an analysis of the experimental RDF can be made by comparison with the calculated one by use of two methods. These are: 1) fitting of the experimental structure function $i(q)$ by adjusting the atomic positions of a selected static model, and 2) calculation of the shape of the $i(q)$ curve by use of the force-field (FF) implemented in the MD scheme; this allows fluctuations in the interatomic distances during the simulation of each chosen model.

Both methods suffer from limitations. The first limitation, in which the static molecular arrangement is subjected to empirical adjustments of the interatomic distances to give the best fit to the measured curve, can produce artefacts, or generate unrealistic structures (e.g., two nonbonded atoms residing at a very short distance or even coinciding). The second method, which avoids the above assumption of a static molecular arrangement, works out the problem by using MD, but this also has a limitation, that is, the calculated shape (peak position and intensity) of the RDF curve does not match the measured one either accurately or entirely. The bias of the latter method clearly depends on the FF used and on the quality of the parameterization for the system dealt with. It follows that the calculated interatomic distances and angles of the model will reproduce those of the material with good approximation, but not exactly.

Currently, the attainment of high-quality molecular structures through accurate MD refinement of the RDFs produced from EDXD measurements is still an issue. Accordingly, in this work we use standard MD simulations with an added biasing potential (see Appendix) to reproduce the experimentally determined curve of the static structure function (SF) $i(q)$. The implemented fitting method was applied and checked for analysis of the EDXD experiments performed on both I and II samples of P-DBNP.

In this study the crystallinity (or lack thereof) of P-DBNP was found to depend upon how the material had been created; both powder (I) and cast-film (II) materials were prepared, each showing different amounts of ordering (vide infra).

Experimental Section

Materials and methods

Samples: The polymer (*R*)-$[NP(O_2C_{20}H_{12})]_n$, a very pale yellow powder, was prepared by the previously described method,[6] but with some modifications. The reaction was carried out in tetrahydrofuran (THF) instead of 1,4-dioxane, the starting $[NPCl_2]_n$ was obtained by the method of Magill,[19] but its solution in THF was made in the presence of solid K_2CO_3, to avoid the formation of poly-THF,[20,21] and, in order to prevent the presence of solvents in the final polymer (these are very easily retained and difficult to remove[6]), the purification was carried out by three consecutive precipitations from THF/water (instead of THF/isopropanol and THF/hexanes) and the product was dried over phosphorous pentoxide in a desiccator at low pressure. Elemental analysis calcd (%) for final product:C 73.0, H 3.67, N 4.25; found: C 71.3, H 3.74, N 4.41. The M_w was 800000 (polydispersity index = 4.6). The specific rotation at 22 °C was $[\alpha]_{Na} = -226°$ (in $CHCl_3$). The ^1H NMR spectrum ($CDCl_3$) showed the expected absence of solvents or water, but the presence of some trimer $[NP(O_2C_{20}H_{12}]_3$. This was confirmed by the ^{31}P NMR spectrum, which allowed a quantitative measurement of 1.5 molecules of

trimer (at 28.0 ppm) per 100 polymeric units (broad signal centred at ≈3 ppm), which means approximately 4% of the trimer by weight.

The polymer film II, pale yellow and fragile, was obtained by slow evaporation of a THF solution of I. The ^{1}H NMR spectrum in $CDCl_3$ showed small retention of THF (0.2 molecules per polymeric unit), which was insufficient for effects to be determined in the RDF curve.

X-ray experiments: Data collection was carried out with a noncommercial X-ray energy-scanning diffractometer[22] suited (fixed θ) to perform energy scanning with a polychromatic X-ray beam and an energy dispersive solid-state detector (SSD) device.

The diffractometer consisted of a Seifert X-ray HV generator supplying a water-cooled tungsten anode (3.0 kW maximum power). The *Bremsstrahlung* component of the X-ray source was used. Operating conditions were: high-voltage supply = 50 kV, current intensity = 40 mA, total power = 2000 W and energy range used = 15.0–40.0 keV.

For diffraction spectra collection, a Ge solid-state detector electronically connected to a multichannel analyser was used. The diffractometer was completed by a set of collimating slits placed in front of and behind the sample. Two-step motors moved the arms, supporting the source and the detector. An adjustable sample holder was placed in the optical centre of the diffractometer. The measurement angles were: θ = 24, 15.5, 8.0, 5.0, 3.0, 2.0, 1.0 and 0.5°.

The calculation of the RDF curves from the q function was described by us previously.[12]

Data analysis

Protocols: The Cerius^2 package developed by BIOSYM/MSI was used to perform all the MM calculations through the OFF (Open Force-field) routine, which includes the empirical functions of the CHARMm force-field.[23] The CHARMm FF parameters were implemented with those previously derived for hexa(aryloxy)phosphazenes.[12] The Crystal facility of this program was used for reproducing the period boundary conditions (PBCs). The atomic charges (P = 1.02, N = −0.35, O = −0.48, C = from −0.03 to 0.08, H = 0.03) were obtained with the charge equilibration method implemented in the Cerius^2 package. The energy-optimized structures were obtained by the conjugate gradient method, satisfying a gradient $\leq$0.1 kJ mol^{-1} Å^{-1}. The scale factor for the nonbonding (NB) 1–4 interactions was set to 0.5. The NB interaction cut-off was implemented by the SPLINE method as a function of the interatomic distance values (r) as follows: for r < SPLINE-ON = 20 Å, fully considered; for r > SPLINE-OFF = 30 Å, fully ignored; for SPLINE-ON < r < SPLINE-OFF, reduced in magnitude. The dielectric constant in the electrostatic function was set as ε = 1.

The MD simulations were carried out by use of a home-made program, which, by using the CHARMm functions, included the bias potential routine (see Appendix). Constant volume and temperature (298 K) ensembles were used for all the calculations. The simulations started from the MM energy-minimised structures. Transients for 5 ps (5000 time steps) with sampling intervals of 0.01 ps were usually collected. The integration time step was 0.001 ps.

Models: Firstly, a single chain of P-DBNP $-R_2PN-$ units was constructed with the aid of some common structural features on chiral polymers provided in the literature.[24,25] A helix conformation of the phosphazene chain has also recently been proposed for the analogous 2,2′-dioxy-diphenyl derivative in solution.[21]

Construction of the initial polymer shape was driven by the following assumptions: 1) for the pure stereoisomer a helix conformational model of the chain should be energetically favoured,[26] and 2) the identity period of two monomeric $-(NPR_2)_2-$ units in the *trans–cis* $[TC]_n$ conformation is established[27] at a close constant value of 4.92 Å (Figure 1). Accordingly, by starting from such a planar $[TC]_n$ backbone, helicoidal chains denoted as A, B, C and D were obtained by $(-R_2PN-)_2$ twist angle values of 10°, 20°, 30° and 60° (number of residues per turn 360° per unit twist; i.e.: 72, 36, 24 and 12). The above conformations correspond to helicoidal turn steps of 175.87, 87.65, 59.28 and 28.84 Å, respectively. Preliminary assay of these single chains in the gas phase by MM calculations showed the C model of the chain to be effectively the most stable, by about 1.5 kcal mol^{-1} per $-R_2PN-$ unit, in the sequence C > B > D > A (Table 1). Such a C-type chain is consistent with a continuous helix with a cylindrical envelope (Figure 2). Subsequent geometry optimization by MM with periodic boundary conditions showed that the hexagonal packing of a C-type helicoidal chain is energetically favoured (by ≈0.6 kcal mol^{-1} per $-R_2PN-$ unit) with respect to that in a tetragonal arrangement (Table 2). Furthermore, the C-type chain in a hexagonal arrangement also had the lowest energy with respect to the B- and D-type chains both in the tetragonal and in the hexagonal packing motifs. Accordingly, to establish the best assembly, length and number of chains suited for reproduction of the experimentally determined RDF, models of P-DBNP were built up exclusively of the C-type chain (here denoted as C(L,N), in which L = length variable up to 20 PN units) packed as N parallel envelopes of helixes (N = 2, 3, 4, 7). The possible relative positionings in blocks of the C-type chains for N = 3, 4 and 7 [C(L,3), C(L,4), C(L,4)′, C(L,4)″ and C(L,7)] were subjected to MD runs (Figure 3).

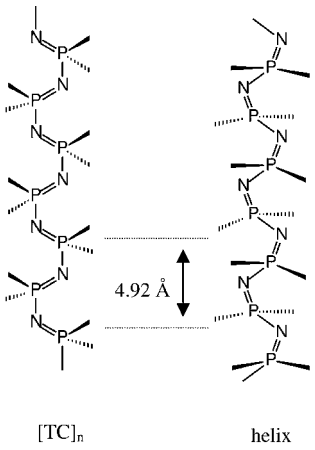

Figure 1. The *trans–cis* $[TC]_n$ and helix conformations of the $(-R_2NP-)_n$ backbone.

Table 1. MM-calculated total energy [kcal mol^{-1} per $-R_2PN-$ unit] for single-chain models A, B, C and D in the gas phase.

Energy	A	B	C	D
bonds	5.130	3.630	3.322	3.100
angles	7.272	5.080	4.453	4.200
torsions	35.886	22.300	23.284	24.874
inversions	0.100	0.060	0.067	0.053
Urey–Bradley	2.838	1.770	1.475	1.500
van der Waals	14.252	9.600	9.050	11.200
electrostatic	−4.360	−2.950	−2.970	−2.600
total energy	61.190	40.040	38.685	42.334

Analogous models were assumed for simulation of the sample of P-DBNP as a cast-film. With it being kept in mind that the experimentally measured RDF of P-DBNP II showed an ordered assembly extending up to about 100 Å, the C-type helix chains had L values extending from 18 to 24 units (maximum length compatible with reasonable computational times).

Results and Discussion

The experimentally identified structure functions (SFs) for the I and II samples of P-DBNP, in the form $q{\cdot}i(q){\cdot}M(q)$, and the RDFs in the DIFF(r) = $D(r)-4\pi r^2\rho_0$ form, obtained from the above SF, are presented in Figure 4. The curve for I (Figure 4a) shows flattened peaks and loss of coherence in the long-distance region (from 30 to 60 Å), thus illustrating the amorphous state of this sample. The curve for II (Figure 4b), in contrast, shows well-defined and regularly spaced peaks over the whole range from 0 to 100 Å, thus indicating

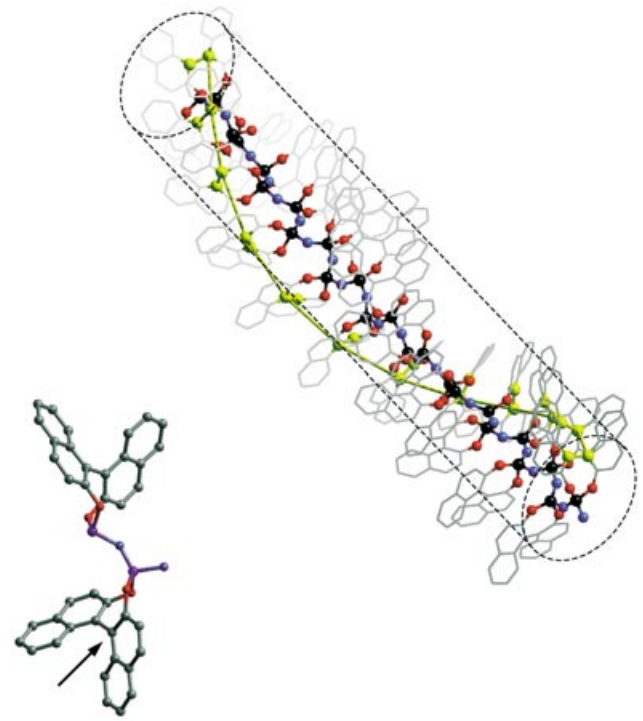

Figure 2. Perspective view of the model of the starting helicoidal structure. The entire turn-step unit is outlined by the solid line that connects the $(-R_2NP-)_n$ backbone through corresponding analogous C atoms (carbon atom denoted by the arrow in the unit of the chain backbone). This atom was selected, instead of an atom of the PN skeleton, for clarity of representation.

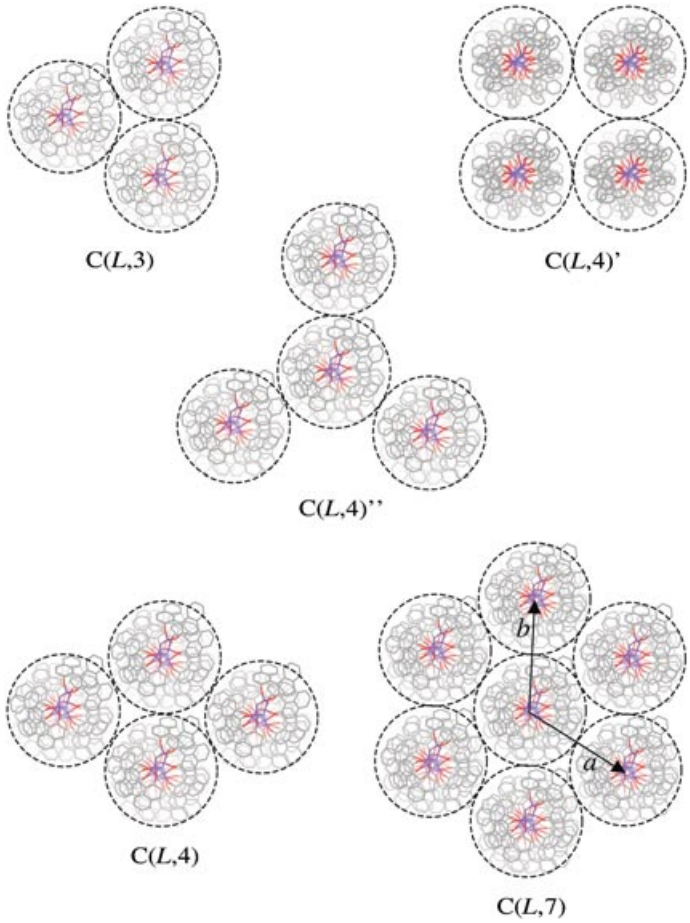

Figure 3. Sections (view from the top) of tubular structures as assembled in the generated models with $N=3$, 4 and 7.

Table 2. MM fully optimised energy [kcal mol^{-1} per $-R_2PN-$ unit] for B-, C- and D-type chains in hexagonal ($a=b=18.9$ Å, $\gamma=120.0°$) and tetragonal ($a=b=18.9$ Å) unit cells, with $c=87.67$ Å (B), $c=59.55$ Å (C) and $c=27.33$ Å (D).

Energy	B		C		D	
	hexagonal	tetragonal	hexagonal	tetragonal	hexagonal	tetragonal
bonds	3.597	3.680	3.339	3.334	3.173	3.168
angles	4.983	5.121	4.407	4.423	4.323	4.303
torsions	23.050	22.867	23.224	23.219	24.523	24.641
inversions	0.054	0.054	0.063	0.064	0.105	0.116
Urey–Bradley	1.760	1.751	1.473	1.459	1.600	1.541
van der Waals	8.057	8.504	7.583	7.980	6.969	7.395
electrostatic	−3.412	−3.147	−3.586	−3.384	−3.229	−3.049
total energy	38.091	38.830	36.503	37.088	37.463	38.115

a much more extended ordered state of the sample. A further important difference is the sharp peak at 2.5 Å^{-1}, reasonably arising from an extended long-distance ordered structure, observable in the ST curve of II and absent in that of I. A feature of the RDF of the powder sample is the deep-intensity negative values of the peaks ranging from about 8 to 18 Å, thus giving rise to a hollow of the curve in this interval. This is attributable to voids inside the material, determined by some change in the torsional angles or, as it is the same, breaking of the chains at the length of about 18 PN units. Furthermore, the RDF peaks of I and II do not coincide significantly by initiating from about 5 Å because of different values in their corresponding interatomic distances. In contrast, the short-distance zones (= 2.5 Å) in both I and II coincide, because this interval reflects bonded atoms (C–H, P–N, P–O, O–C, C–C…) and close-lying non-bonded atoms (e.g., N···O, N···N, O···O, O···P, O···C…) in the common $-R_2PN-$ unit.

MD simulations implementing the biasing potential method described in the Appendix section were used to calculate theoretical RDFs. All the single- or double-chain ($N=1$ and 2) models with L varying from 10 to 20 were ruled out on the basis of significant disagreement between the experimentally determined RDFs and the calculated ones. The theoretical SFs and RDFs found for the remaining selected models C(18,3), C(18,4) and C(18,7), characterised by arrangements (Figure 3) of three, four and seven chains as tubular structures, respectively, gave good selective agreement with the corresponding experimentally determined curve for I (Figure 5a–c). For brevity they are therefore considered from here onwards. The most important feature that allowed us to discriminate between the best three models was the agreement factor (χ^2) between the points of the ex-

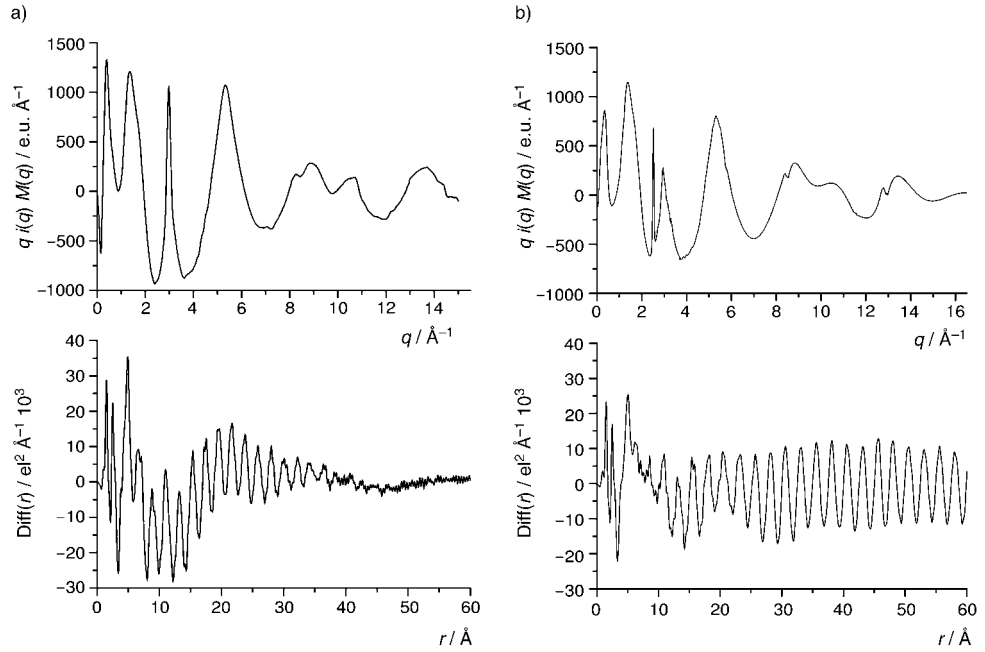

Figure 4. The observed (LAXS) structure functions (top) and the associated RDFs (bottom) for a) P-DBNP bulk and b) film.

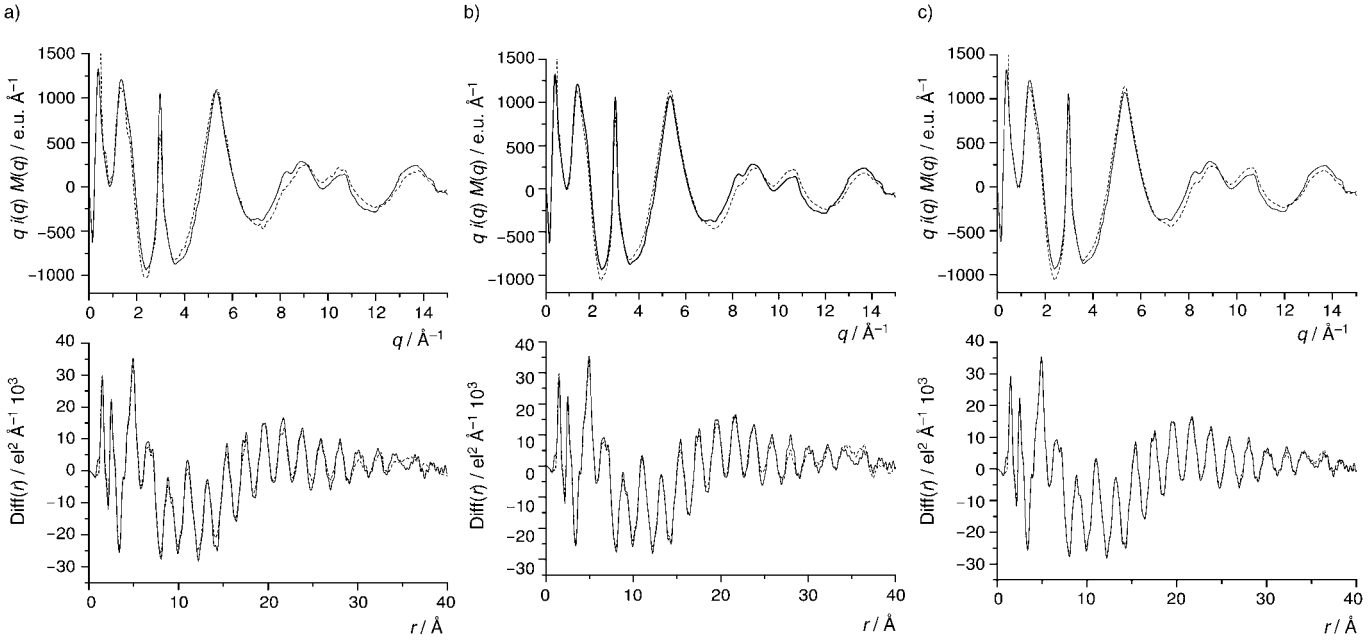

Figure 5. Comparison between observed (solid line) and MD-calculated (dotted line) structure functions (top) and related RDFs (bottom) for the a) C(18,3), b) C(18,4) and c) C(18,7) models of P-DBNP in the bulk state.

perimentally observed and the theoretical RDF curves. The attained χ^2 values were 1.494, 1.617 and 0.816 for the models C(18,3), C(18,4) and C(18,7), respectively, thus showing that the last was the best model. Comparisons based on Figure 5a–c also showed that the calculated RDF for C(18,7) almost perfectly reproduced both position and intensity of the peaks up to 30 Å (Figure 5c), whereas this is not the case for C(18,3) and C(18,4). These last two models agree less exactly, than in the case of the model C(18,7), for the shapes and intensities of some peaks in the 0–30 Å range, and in particular in the zone of the low-intensity peaks (30–37 Å) preceding the loss of coherence. Elongation of the chain had no effect on the simulated curve of the model, thus indicating that the ordering of the chains is interrupted at an L value >18 by some conformational transition or by chain-breaking.

The best agreement between theoretical and measured RDF curves (Figure 6) was attained for P-DBNP II assembled in the analogous, but more elongated, C(24,7) hexagonal model. In this case, the increased length (24 units) of the

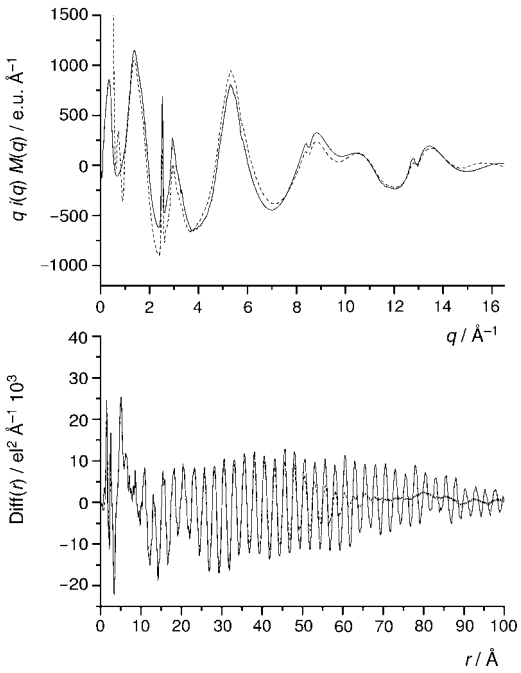

Figure 6. Comparison between observed (solid line) and MD calculated (dotted line) structure functions (top) and related RDF (bottom) for the P-DBNP as-cast film II.

simulated seven chains allowed the RDF shape to be reproduced fairly well up to 37 Å. At distances >37 Å (from 38 to 100 Å) the calculated peak positions match well with the experimentally observed values, but the intensities decrease gradually to zero with increasing distances. This confirmed the expected more extended order in the film with respect to that in the powder, thus also suggesting that the shape of the whole RDF curve may be completely reproducible through simulation of a C(L,7) model after a further elongation (>100 Å) of the polymer chain along the c axis (i.e., until $L=50$). A check of this expectable result is not possible with our computing resources, because it requires an extremely long time for computations, further made more demanding by the bias potential used.

Effective packing forces seem to be responsible for the observed predominant hexagonal seven-chain C(L,7) assembly of the polymer in the bulk state. This assembly can be accounted for by the diminution in entropy due to the more symmetric and ordered arrangement attained in the solid by adjacent cylindrical envelopes of the isochiral chains. Interestingly, the ratios of N to number of voids decrease in the order 4, 3, 2, 1.16_6 for the models C(18,4), C(18,3), C(18,4)′ and C(18,7), respectively. The predominating packing of seven cylindrical envelopes can thus be safely explained in terms of the best quantity and symmetry of the voids useful for determining the maximum covering surface of the assembled material (Figure 3). In fact, the observed trend in the ratios of N to number of voids is consistent with the MM-calculated total energies of the corresponding models (Table 3). This table also shows that the energy contribution favouring the seven-chain arrangement is derived in part from the nonbonding van der Waals and electrostatic terms. This finding is thus consistent with an entropic factor determining the predominance of the above assembly both in I and in II.

Table 3. MM fully optimised energies [kcal mol^{-1} per $-R_2PN-$ unit] in the gas phase for the C(L,N) models at various N values (Figure 3). The chain length L was fixed at the value $L=24$ needed to obtain a complete helix turn.

Energy	C(24, 3)	C(24,4)	C(24,4)′	C(24,7)
bonds	3.294	3.304	3.334	3.312
angles	4.423	4.409	4.423	4.401
torsions	23.221	23.218	23.219	23.225
inversions	0.066	0.064	0.064	0.064
Urey–Bradley	1.472	1.469	1.453	1.471
van der Waals	8.489	8.391	8.471	8.188
electrostatic	−3.114	−3.174	−3.167	−3.277
total energy	37.809	37.682	37.797	37.383

Table 4 shows the bond lengths and angles obtained from the MD simulations of I and II, each sampled as the average of the averaged values along each chain of the model.

Table 4. Averaged values of selected bond lengths [Å] and angles [°] for P-DBNP I and II as obtained from MD simulations as last 3000 time steps of the C(18,7) and C(24,7) models, respectively.

	C(18,7)	C(24,7)
P–N	1.636	1.645
P=N	1.567	1.565
P–O	1.615	1.646
O–C	1.400	1.414
P–N–P	138.303	142.784
N–P–N	106.310	111.466
N–P–O	104.917	102.717
N=P–O	119.399	118.532
P–O–C	126.199	122.989
N–P=N–P	−154.85	−179.47
P–N=P–O1	−34.66	−54.96
P–N=P–O2	90.68	66.92
N=P–N=P	0.69	14.45
P=N–P–O1	−126.88	−115.73
P=N–P–O2	125.00	141.28

Both the intra- (P–N and P=N), and extra-chain (P–O and O–C) bond lengths are scarcely affected on passing from I to II. The P–N and P=N bond lengths range approximately from 1.636 to 1.645 Å, and from 1.567 to 1.565 Å, respectively. This alternate single–double PN bond length character is consistent with results from previous reports.[12,28,29] The P–O and O–C bond lengths fall in the range of X-ray-determined values for two tris-spirocyclophosphazenes bearing three 2,2′-dioxy-binaphthyl and 2,2′-dioxy-biphenyl groups.[14,30]

The sets of bond angles for I and II show relative differences spanning a range from a minimum of 0.9° (N=P–O) to a maximum of 5.15° (N–P–N). In both I and II the chain backbone fluctuates about the PN single bond dihedral by approximately ±5–7°, while the N–P=N–P torsional angles have scarcely moved (ca. ±7–5°) on the picosecond timescale. The torsional angles about PN double and single bonds (Table 4) revealed a more significant variation on passing from I to II as an effect of the casting of the materi-

al. This made the effect of the microscopic structure on the backbone conformation observable and determinable. In fact, the larger (by ca. 25°) P–N=P–N torsional angle corresponds to a more flattened conformation of the chain; that is, a helix with a slightly distorted *cis–trans* conformation, in the cast-film sample II. The structural and conformational modification between I and II arising from their different torsion angles was that the corresponding repeat distances of the $-(R_2PN)_2-$ pair are different, namely 4.35 and 4.96 Å, in I and II, respectively (Figure 7).

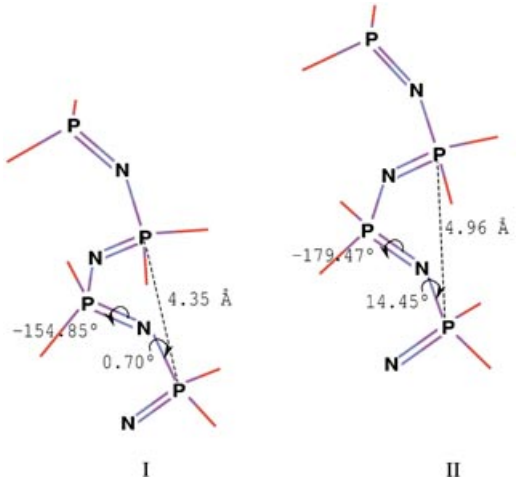

Figure 7. Schematic representation of the modification of the P-DBNP sample I into II. The repetition step along the backbone [Å] and the torsional angles [°] are averages of the last 3000 time steps of the MD simulations of the models C(18,7) (I) and C(24,7) (II).

The results found are in line with previous general symmetry and energy considerations on isochiral chain packing,[24] which suggest that ordered hexagonal structures of the helix chains are likely for chiral polymers. Recent data on the effect of temperature on the molecular weight and on the specific rotation of isotactic binaphthoxy derivatives in solution[6–8] are consistent with a helix conformation of the P–DBNP chains. This feature of P-DBNP in solution is common to a novel type of interesting synthetic optically active polymers (SOAPs).[10]

Inclusion of the bias potential in the simulations produced an accurate reproduction of the experimentally observed RDF for the best model. Consequently, otherwise unattainable reliable structural information was derived in both the static and dynamic analyses of the RDF curve. The inclusion of the biasing routine, however, caused an increase of the calculation time by a factor of 10^3. On the other hand, a corresponding diminution of the evolution time needed for convergence was observed when a force field (FF) integrated with the bias potential was used. Table 5 presents data showing the attainment of the best total energy for the models through the use of the FF including the bias potential instead of the pure FF. In this latter case much longer MD evolution times were needed for higher relative energy to be reached.

Table 5. Comparison of the average energies [kcal mol^{-1} per $-R_2PN-$ unit] obtained from simulations of the C(L,7) models of I and II (with $L=18$ and $L=24$, respectively) with included (FF+b) and excluded (FF) bias potential.

FF Energy terms	FF+b (I)	FF+b (II)	FF
bonds	16.367	14.682	21.158
angles	14.435	13.536	18.867
torsions	26.931	25.308	24.881
inversions	2.725	2.271	4.772
Urey–Bradley	4.633	3.712	3.750
van der Waals	11.978	11.715	12.347
electrostatic	−4.102	−4.409	−4.164
total energy	72.965	66.814	81.608

Conclusion

The structure and molecular assembly of the amorphous P-DBNP, both as a powder (I) and as a cast-film (II), was studied by a combined experimental (LAXS) and computational (MD) approach, implemented here by the use of a biasing potential in the MD simulations, from which the theoretical RDFs for a given model were calculated. The bias achieved more accurate reproduction of the experimentally measured curve for the best model than was seen when the bias was omitted, thus making the approach more convenient for structural information on the amorphous material and for better accuracy of the structural data. The machine time required by the computations was increased (by a factor of ca. 10^3) after the inclusion of the bias potential routine, but this disadvantage was counterbalanced by lower evolution times of the simulations in locating the best RDF. The model that best matches the computed and the experimentally determined RDF curves for I and II consists of seven hexagonal helix chains assembled in a parallel fashion. MM calculations confirmed such a packing to be energetically favoured. The LAXS curves showed that maximum lengths attainable by the tubular helicoidal chains of P-DBNP were about 30 Å and 100 Å in I and II, respectively. Important structural information concerning I and II was revealed: 1) the flattening of the chain backbone when the material is as-cast film, and 2) the consequent different distances assumed by the identity period of the two monomeric units $(-R_2NP-)_2$ in I (4.35 Å) and in II (4.96 Å) (Figure 7). The biasing routine provided MD runs resulting in models with lower energies than those attainable by MD with FF without the use of the bias potential routine.

In conclusion, the approach used has demonstrated the capability to distinguish inter- and intrachain modifications of the material with good accuracy on going from the bulk to the as-cast film. This result is in general suited to provide key information on the effects of the preparation conditions on the structure and technologically important physical properties that may be shown by samples of an amorphous material. The MD technique implemented by the bias potential allowed a better analysis of the RDF curve obtained from X-ray scattering data, thus making the approach applicable to the deduction of new quantitative structural information on polyphosphazenic materials regardless of their degree of crystallinity.

Appendix

In a force field (FF)[31] at the lowest order of approximation, the potential energy is assumed to be the sum of single energy terms, each of which is a function of a "chemical" valence coordinate [Eq. (1)].

$$E_{FF} = \sum_{\text{bond stretching}} U_b(b) + \sum_{\text{angle bending}} U_\theta(\theta) + \sum_{\text{dihedral angles}} U_\tau(\tau) + \ldots + \sum_{\text{nonbonding distances}} U_{nb}(r) \quad (1)$$

For example, $U_b(b)$ is the function that takes account of the stored amount of energy in the stretching of a bond. This equation is just an approximation, though a very good one, of the real potential energy of the whole system. Neglected here are all those interactions that are usually small in value and have a complicated functional form, and those interactions which depend on the particular chemical environment. For this reason, FFs usually give results with slight discrepancies with respect to experimentally observed data.

In order to obtain results that better match the experiments, some of the neglected terms should be taken into account. The problem is to identify which terms are really important and to give them the right weight with respect to all the others.

To avoid this task, all these interactions can be considered in a biasing potential, which modifies the system's potential energy hypersurface by taking account of discrepancies with some ad hoc experimental measurements. This can be done if the experimental data can be cast in terms of the atomic coordinates, so that the additional energy term will be a function of the coordinates, and the form can be, as in a best-fit procedure, the χ^2 function.

In the best-fit procedure, the main task is to minimize the χ^2 function (that is, the sum of the squares of the differences between the experimentally measured points and the theoretically calculated ones) in order to obtain all the parameters involved by the model.

In the case of coherent scattering of X-rays from an ensemble of atoms, the intensity of the scattered wave is a function of the distance between every pair of atoms present in the ensemble [Eq. (2)]:

$$i_{theor}(q) = \sum f_j f_k \frac{\sin(r_{jk}\, q)}{r_{jk}\, q} \quad (2)$$

in which r_{jk} is the distance between atom j and atom k, f_j and f_k are the scattering factors for these two atoms, and q is the scattering parameter, which depends on λ (the wavelength of the X photon) and θ (the scattering angle), $q = (4\pi/\lambda)(\sin\theta)$.

The χ^2 value is hence a function of the atom positions, and it can be assumed that the biasing potential (or energy term) is proportional to this value. The total energy of the system is now $E_{TOT} = E_{FF} + E_{\chi^2}$. E_{χ^2} is defined in Equation (3):

$$E_{\chi^2} = K_{\chi^2} \sum_{i=1}^{N} [i_{exptl}(q_i) - i_{theor}(q_i)^2] \quad (3)$$

in which K_{χ^2} is a scaling constant with dimensions of an energy. All the terms included in E_{TOT} are functions of atomic coordinates. The contributing forces (E_{χ^2}) that act on an atom j are, of course, to be added to the FF-calculated forces [Eq. (4)]

$$\vec{F}_j = -\frac{dE}{d\vec{r}_j} = -\frac{dE_{FF}}{d\vec{r}_j} - \frac{dE_{\chi^2}}{d\vec{r}_j} \quad (4)$$

Acknowledgments

This work was supported by the Italian MIUR (PRIN 2002–4) and the Spanish FYCYT (project PB-EXP01–15) and MEC (BQU-2001–3676). G.C.P. is grateful to Professor K. B. Lipkowitz for discussions and suggestions concerning the manuscript. Thanks are also due to Professor Ruggero Caminiti for making EDXD measurements possible.

[1] C. W. Allen, *Coord. Chem. Rev.* **1994**, *130*, 137–173.
[2] R. De Jaeger, M. Gleria, *Prog. Polym. Sci.* **1998**, *23*, 179–276.
[3] *Phosphazenes: A Worldwide Insight* (Eds.: R. De Jaeger, M. Gleria), NOVA Science, New York, NY, **2003**.
[4] *Chemistry and Applications of Polyphosphazenes*, (Ed.: H. R. Allcock), Wiley, New York, NY, **2002**.
[5] G. A. Carriedo, L. Fernández-Catuxo, F. J. García Alonso, P. Gómez-Elipe, P. A. González, *Macromolecules* **1996**, *29*, 5320–5325.
[6] G. A. Carriedo, F. J. García Alonso, P. A. González, J. L. García Alvarez, *Macromolecules* **1998**, *31*, 3189–3196.
[7] G. A. Carriedo, F. J. García Alonso, P. Gómez Elipe, J. L. García Alvarez, M. P. Tarazona, M. Teresa Rodriguez, E. Sáiz, J. T. Vázquez, J. I. Padrón, *Macromolecules* **2000**, *33*, 3671–3679.
[8] G. A. Carriedo, P. Crochet, F. J. García Alonso, J. Gimeno, A. Presa, *Eur. J. Inorg. Chem.* **2004**, in press.
[9] G. A. Carriedo, F. J. García Alonso, A. Presa, *Eur. J. Inorg. Chem.* **2003**, 4341–4346.
[10] T. Nakano, Y. Okamoto, *Chem. Rev.* **2001**, *101*, 4013–4038.
[11] S. D. Dreher, T. J. Katz, K. C. Lam, A. L. Reingold, *J. Org. Chem.* **2000**, *65*, 815–822.
[12] R. Caminiti, M. Gleria, K. B. Lipkowitz, G. M. Lombardo, G. C. Pappalardo, *J. Am. Chem. Soc.* **1997**, *119*, 2196–2204.
[13] R. Caminiti, M. Gleria, K. B. Lipkowitz, G. M. Lombardo, G. C. Pappalardo, *Chem. Mater.* **1999**, *11*, 1492–1497.
[14] M. E. Amato, R. Caminiti, G. A. Carriedo, F. J. García Alonso, J. L. García Alvarez, G. M. Lombardo, G. C. Pappalardo, *Chem. Eur. J.* **2001**, *7*, 1486–1494.
[15] M. E. Amato, G. A. Carriedo, F. J. García Alonso, J. L. García Alvarez, G. M. Lombardo, G. C. Pappalardo, *J. Chem. Soc. Dalton Trans.* **2002**, 3047–3053.
[16] T. Egami, H. J. Gunterodt, H. Beck, *Glassy Metals*, *Vol. 1*, Springer, Berlin **1981**, pp. 25–61.
[17] K. Nishikawa, T. Iijima, *Bull. Chem. Soc. Jpn.* **1984**, *57*, 1750–1759.
[18] V. Rossi Albertini, L. Bencivenni, R. Caminiti, F. Cilloco, C. Sadun, *J. Macromol. Sci. Phys.* **1996**, 35, 199–213.
[19] A. N. Mujumdar, S. G. Young, R. L. Merker, J. H. Magill, *Macromolecules* **1990**, *23*, 14–21.
[20] G. A. Carriedo, F. J. García Alonso, P. Gómez Elipe, P. A. González, C. Marco, M. A. Gómez, G. Ellis, *J. Appl. Polym. Sci.* **2000**, *77*, 568–576.
[21] M. T. R. Laguna, M. P. Tarazona, G. A. Carriedo, F. J. García Alonso, J. I. Fidalgo, E. Sáiz, *Macromolecules* **2002**, *35*, 7505–7515.
[22] R. Caminiti, C. Sadun, V. Rossi, F. Cilloco, R. Felici, It. Patent no. RM/93 01261484, **1993**, June 23.
[23] B. R. Brooks, R. E. Bruccoleri, B. D. Olafson, D. J. States, S. Swaminathan, M. Karplus, *J. Comput. Chem.* **1983**, *4*, 187–217.
[24] S. V. Meille, G. Allegra, *Macromolecules* **1995**, *28*, 7764–7769.
[25] H. R. Allcock, R. L. Kugel, E. G. Stroh, *Inorg. Chem.* **1972**, *11*, 1120–1123.
[26] R. C. Boehm, *J. Phys. Chem.* **1993**, *97*, 13877–13886.
[27] E. Giglio, F. Pompa, A. Ripamonti, *J. Polym. Sci.* **1962**, 59, 293–300.
[28] C. W. Burkhart, P. C. Gillette, J. B. Lando, J. J. Beres, *J. Polym. Sci. Polym. Chem. Ed.* **1983**, *21*, 2349–2363.
[29] Y. Chatani, K. Yatsuyamagi, *Macromolecules* **1987**, *20*, 1042–1045
[30] H. R. Allcock, M. T. Stein, J. A. Stanko, *J. Am. Chem. Soc.* **1971**, *93*, 3173–3178
[31] U. Burkert, N. L. Allinger, *Molecular Mechanics*, ACS Monograph 177, ACS, Washington, DC, **1982**.

Received: January 16, 2004
Published online: June 15, 2004

